THE INFLUENCE OF THE LENGTH-TO-DIAMETER RATIO ON TWO-PHASE FLOW DISTRIBUTION AND STABILITY IN MICROCHANNELS UNDER ENTRANCE EFFECTS

Yuan-Hang LI *

School of Mechanical Engineering, Shanghai Institute of Technology, Shanghai, China

* Corresponding author; E-mail: yh0588a@163.com

Entrance effects are a key factor governing the stability and flow maldistribution in parallel microchannels. In this study, a flow model that accounts for the entrance-region friction factor is developed to characterize how developing flow in the entrance section influences the pressure-drop–flow-rate characteristics of an individual channel and the operating point of the parallel system. On this basis, the role of entrance effects in regulating the stability range and flow distribution uniformity of parallel microchannels is systematically investigated. Furthermore, the length-to-diameter ratio is introduced as a critical geometric parameter to examine its influence on system behavior under different length-to-diameter ratio. The results show that decreasing the length-to-diameter ratio significantly increases the fraction of the entrance region relative to the total channel length, thereby strengthening the flow-resistance augmentation induced by entrance effects. Consequently, the instability range of the parallel system is effectively narrowed, inter-channel flow redistribution is suppressed, and the degree of flow maldistribution is reduced.

Key words: *microchannel, entrance effects, flow distribution, stability*

1. Introduction

Microchannel heat sinks, benefiting from their high surface-area-to-volume ratio and enhanced heat transfer capability, show strong potential for thermal management of high-heat-flux electronic devices [1-3]. In parallel microchannel systems, flow maldistribution and flow instability are two key issues that strongly affect thermal performance and operational safety. Flow maldistribution refers to the unequal distribution of mass flow rate among parallel channels, which may cause insufficient cooling in low-flow channels and increase the risk of local dryout and overheating. Under two-phase conditions, parallel channels are also susceptible to flow instabilities. Ledinegg instability is a static instability associated with the negative slope of the pressure drop – flow rate curve, and it may trigger sudden flow redistribution among channels. Experimental measurements showed that significant flow maldistribution can occur in parallel microchannel heat sinks due to non-uniform pressure distribution in the inlet and outlet manifolds [4]. Experimental studies showed that flow stability in microchannel heat sinks is strongly influenced by pressure drop characteristics and channel geometry, which also affect flow distribution among channels [5]. This review summarized flow boiling mechanisms, pressure drop models, and flow instability phenomena in microscale channels, and highlighted the strong coupling between pressure drop and flow distribution [6]. Several previous studies [7-14] have investigated flow and heat transfer phenomena in microchannels, which may provide useful guidance

for modeling assumptions and parameter selection. These works offer general references for the analysis of flow distribution and related parameter considerations.

However, most existing studies on microchannels are conducted under the assumption of fully developed flow. In both experiments and numerical simulations, the influence of entrance effects is often weakened or avoided by extending the upstream flow section before the heated region, thereby simplifying the analysis of pressure drop and heat-transfer characteristics. In reality, at the microscale, the entrance region can account for a considerable portion of the total channel length, and the development of hydrodynamic and thermal boundary layers can significantly alter local frictional resistance and heat transfer [15-17]. Previous studies have shown that both hydrodynamic and thermal entrance effects significantly influence pressure drop and heat transfer characteristics in rectangular microchannels, especially when the channel length is short [18]. Some researchers investigated the hydrodynamic entrance length in rectangular microchannels and showed that the developing region may occupy a significant portion of the channel length, and ignoring entrance effects may lead to inaccurate prediction of pressure drop [19]. Morini reviewed single-phase flow and heat transfer in microchannels and pointed out that developing flow and entrance effects play an important role in determining friction factor and heat transfer characteristics in short microchannels [20]. Qu and Mudawar showed that the hydrodynamic and thermal developing regions may occupy a significant portion of the microchannel length, and therefore developing flow effects must be considered in pressure drop and heat transfer analysis [21]. Kandlikar pointed out that in microchannels the entrance region can occupy a large portion of the total channel length, and the assumption of fully developed flow may lead to significant errors in pressure drop prediction [22].

Although studies on entrance effects in microchannel heat transfer are limited, some investigations have demonstrated that entrance effects have a significant influence on heat transfer within microchannels. Since pressure drop characteristics determine the operating point and flow distribution in parallel channels, the entrance effect may further influence flow maldistribution and flow instability in parallel microchannel systems. Therefore, it is necessary to investigate microchannel flow and heat transfer with entrance effects taken into account.

2. Modeling approach

2.1. Problem Description

Figure 1 schematically illustrates the flow configuration of a parallel microchannel system. The working fluid is delivered by a pump to a set of microchannels arranged in parallel with a common inlet manifold and then discharged through a common outlet manifold. Each microchannel has a height H_c = 0.2 mm, a width W_c = 0.2 mm, and a length L_c = 10 mm. A heat source is applied beneath the microchannels, causing the fluid to be heated and potentially evaporate as it flows downstream. Depending on the heating intensity, inlet subcooling, and channel geometric parameters, the outlet condition may remain single-phase liquid, transition to two-phase flow, or become predominantly vapor.

To account for entrance effects, a developing-flow friction factor is employed for the inlet region, whereas the fully developed friction factor is used for the remaining portion of the channel. In contrast, when entrance effects are neglected, the fully developed friction factor is applied over the entire channel length.

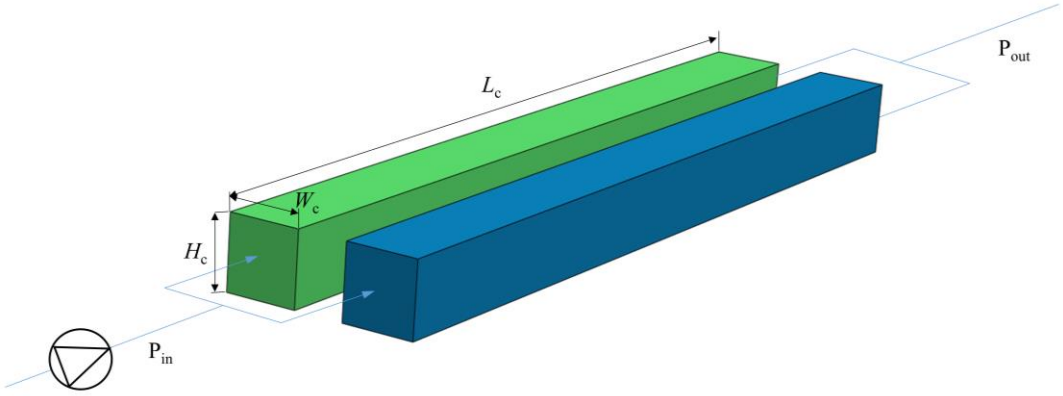

Figure 1. Schematic diagram of the parallel microchannel system layout

2.2. Dynamic flow network equations

Due to the horizontal placement of the microchannel heat exchanger, the gravitational pressure drop can be neglected. The subcooled working fluid enters the microchannel and flows under the driving pressure head.

The momentum equation for each channel is given by the following equation:

$$m_i \frac{dW_i}{dt} = -f_i(W_i) + \Delta p \tag{1}$$

This equation governs the time evolution of the mass flow rate W_i in each channel. The steady-state pressure drop, as a function of flow rate, i.e., the channel load curve, is given by $f_i(W_i)$. When the actual pressure drop $\Delta p = p_{in} - p_{out}$ across the channel deviates from the steady-state pressure drop $f_i(W_i)$ corresponding to the current flow rate, the channel flow rate W_i changes with time. The inertia coefficient m is a parameter that characterizes the speed of the channel's response to flow rate changes. Its physical meaning is the ratio of the channel length L_c to the cross-sectional area A_c.

In the idealized open-loop flow network considered here, the pressure drop Δp equals the pump head only in steady-state conditions and only if all other upstream and downstream flow resistances in the flow circuit with the parallel flow channels are neglected.

The pump curve is given by the following equation:

$$0 = F_p(W, \Delta p) \tag{2}$$

The implicit function $F_P(W, \Delta p)$ specifies the relationship between the pump flow rate W and the pressure drop Δp.

The law of mass conservation states that the pump flow rate W equals the sum of flow rates W_i in each channel:

$$0 = \left(\sum_{i=1}^{N} W_i \right) - W \tag{3}$$

Where N is the number of channels, and W is also referred to as the total flow rate.

The pressure drop model is used to calculate the steady-state channel load curve. The load curve for a single channel is given by the following equation:

$$\Delta p = f_i(W_i) = p_{in} - p_{out} \tag{4}$$

The pressure drop model is based on the assumption of separated flow, with local thermal equilibrium between phases, meaning that the phases are distinct and have different properties. There may be velocity slip between the phases, but no temperature difference. We use a one-dimensional method, where properties vary only in the flow direction.

The flow of the liquid-vapor mixture is governed by the following conservation equations:

Mass conservation:

$$\frac{\partial G}{\partial z} = 0 \tag{5}$$

Momentum conservation:

$$\frac{\partial}{\partial z}\left[\left(v_{\mathrm{f}}\frac{(1-x)^2}{1-\alpha}+v_{\mathrm{g}}\frac{x^2}{\alpha}\right)G^2\right] = -\frac{\partial p}{\partial z} - F_{\mathrm{w}} \tag{6}$$

Energy conservation:

$$\frac{\partial}{\partial z}(hG) = \frac{Q'}{A_{\mathrm{c}}} \tag{7}$$

Assuming that the contributions of gravity and potential energy can be neglected, these assumptions are typically applicable to heated flow in rectangular microchannels. For simplicity, the heat generated by viscous dissipation is excluded.

The main variables in these equations are G (the mass flux), p (the pressure), and h (the enthalpy). Three boundary conditions are used to solve these first-order differential equations:

The inlet boundary condition for the mass flux is given by:

$$G_i\big|_{z=0} = G_{\mathrm{in},i} \tag{8}$$

The outlet boundary condition for pressure is given by:

$$p_i\big|_{z=L_{\mathrm{c}}} = p_{\mathrm{out}} \tag{9}$$

The inlet boundary condition for enthalpy is given by:

$$T_{\mathrm{f},i}\big|_{z=0} = T_{\mathrm{in}} \Rightarrow h_{\mathrm{f},i}\big|_{z=0} = h(T_{\mathrm{in}}, p(0)) \tag{10}$$

The following secondary variables are required to fully close the system of equations.

The thermodynamic equilibrium quality x_{eq}:

$$x_{\mathrm{eq}} = \frac{h-h_{\mathrm{f}}}{h_{\mathrm{g}}-h_{\mathrm{f}}} \tag{11}$$

The steam quality x represents the proportion of vapor in a liquid-vapor mixture. To ensure physical meaning, its value must be constrained between [0, 1], where:

$$x = P_{[0,1]}\left(x_{\mathrm{eq}}\right) \tag{12}$$

The void fraction in the bubbly flow α:

$$\alpha = \frac{1}{1+\frac{v_{\mathrm{f}}}{v_{\mathrm{g}}}S\frac{1-x}{x}} \tag{13}$$

The slip ratio S is a parameter that describes the relative velocity difference between the liquid and vapor phases in the flow. It is commonly estimated using empirical correlations. In this case, the slip ratio S is estimated using the Zivi correlation [23], which is given by:

$$S = \left(\frac{v_g}{v_f} \right)^{\frac{1}{3}} \tag{14}$$

The frictional pressure drop F_w is calculated using empirical correlations. In this study, the frictional pressure drop is estimated using the classical Lockhart-Martinelli method [24], combined with the modified correlation proposed by Chisholm [25] to improve the accuracy of predictions. We adopt the formalized expression introduced by Muzychka and Awad [26], which makes the model more practical and versatile for engineering applications.

$$F_w = \left(\frac{\partial p}{\partial z} \right)_f + C \sqrt{\left(\frac{\partial p}{\partial z} \right)_f \left(\frac{\partial p}{\partial z} \right)_g} + \left(\frac{\partial p}{\partial z} \right)_g \tag{15}$$

The Chisholm constant C is used to quantitatively describe the strength of the interaction between the liquid and vapor phases during two-phase flow. When both phases are in laminar flow, the empirical value for C is taken as 5 [25]. In the calculation of single-phase frictional pressure drop, it is typically assumed that the liquid or vapor fully occupies the cross-sectional area of the pipe, meaning that when calculating the pressure drop for one phase, the presence of the other phase is ignored. This simplification reduces the complexity of two-phase flow while also providing a reasonable physical basis for the construction of empirical models. This assumption allows for easier modeling of each phase's behavior and is widely used in practical engineering applications where precise two-phase models may be difficult to implement.

$$\left(\frac{\partial p}{\partial z} \right)_f = 2 f_f \frac{v_f (1-x)^2 G^2}{D_h} \tag{16}$$

$$\left(\frac{\partial p}{\partial z} \right)_g = 2 f_g \frac{v_g x^2 G^2}{D_h} \tag{17}$$

Under the condition of fully developed laminar flow, the single-phase friction factor f in a rectangular channel can be calculated using the following formula [27]:

$$f\,\mathrm{Re} = 24\left(1 - 1.3553\beta + 1.9467\beta^2 - 1.7012\beta^3 + 0.9564\beta^4 - 0.2537\beta^5\right) \tag{18}$$

Under the condition of developing laminar flow, the single-phase friction factor f_A in a rectangular channel can be calculated using the following formula [28]:

$$f_A\,\mathrm{Re} = \frac{3.44}{\sqrt{x^+}} + \frac{(f\,\mathrm{Re}) + \frac{K(\infty)}{4x^+} - \frac{3.44}{\sqrt{x^+}}}{1 + C_A (x^+)^{-2}} \tag{19}$$

The dimensionless hydrodynamic length, denoted as x^+:

$$x^+ = \frac{x}{D_h\,\mathrm{Re}} \tag{20}$$

In two-phase flow, the flow characteristics of the liquid and vapor phases differ significantly. Therefore, when evaluating the flow regime, the Reynolds number for each phase should be calculated separately.

$$\mathrm{Re}_{\mathrm{f}} = \frac{(1-x)GD_{\mathrm{h}}}{\mu_{\mathrm{f}}} \tag{21}$$

$$\mathrm{Re}_{\mathrm{g}} = \frac{xGD_{\mathrm{h}}}{\mu_{\mathrm{g}}} \tag{22}$$

In the entrance region, due to the large velocity and pressure gradients, the pressure drop caused by developing flow is significantly higher than that of fully developed flow. Therefore, there exists a clear length boundary between the developing flow and the fully developed flow state, which serves as the basis for the separation of the use of different friction factors. The estimation of the entrance length is based on the empirical correlation proposed by Duan et al. [16], which is used to reasonably define the range of the developing flow influence in microchannels, thereby improving the accuracy of pressure drop predictions.

$$L_{\mathrm{e}} = \left(\frac{0.74}{0.09\mathrm{Re}+1} + 0.0889\mathrm{Re} \right) D_{\mathrm{h}} \tag{23}$$

2.3. Steady-state flow distributions

The cumulative load curve for the entire parallel channel array is constructed. This curve is obtained by summing the flow rates of all channels at a given pressure drop Δp. Since the load curve of each heated channel typically exhibits an N-shaped characteristic, it means that at a certain pressure drop value, there could be three different flow rates corresponding to the same pressure drop. Therefore, at a given pressure drop Δp, the system may have up to 3^N different flow combinations (each channel having three flow choices, with a total of N channels).

In principle, the system's steady-state operating point occurs only at the intersection of the cumulative load curve and the pump characteristic curve. However, since the specific form of the pump curve can be arbitrary, every point on the cumulative load curve could potentially become the system's operating point under a certain pump characteristic curve. To maintain general applicability, this study will not be limited to a specific pump curve but will instead discuss the properties of the entire cumulative load curve.

2.4. Stability analysis

To determine whether the steady-state operating point can be achieved in practice, we need to evaluate its stability. We conduct a stability analysis of the system dynamics, which is based on the linearization of the system equations (1) to (3). The linearized system can be represented as:

$$\begin{bmatrix} m_1 & & & \\ & m_2 & & \\ & & 0 & \\ & & & 0 \end{bmatrix} \cdot \frac{d}{dt} \begin{bmatrix} \delta W_1 \\ \delta W_2 \\ \delta W \\ \delta(\Delta p) \end{bmatrix} = \begin{bmatrix} -\varepsilon_1 & & & 1 \\ & -\varepsilon_2 & & 1 \\ & & \varepsilon_W & \varepsilon_{\Delta p} \\ 1 & 1 & -1 & 0 \end{bmatrix} \cdot \begin{bmatrix} \delta W_1 \\ \delta W_2 \\ \delta W \\ \delta(\Delta p) \end{bmatrix} \tag{24}$$

By linearizing the system, we simplify its nonlinear behavior into an approximate linear system. This simplification allows us to evaluate the system's behavior near the steady-state operating point. The linearized system provides the response to small deviations, which is crucial for determining whether the system can maintain stability.

In analyzing the system, the symbol δ is used to represent small deviations of the system from the steady-state operating point. By studying the effects of these small changes on the system, we can better understand its dynamic characteristics. To simplify the expression, we introduce the following symbols to represent partial derivatives:

$$\varepsilon_i = \frac{\partial f_i}{\partial W_i} \tag{25}$$

$$\varepsilon_W = \frac{\partial F_{\mathrm{p}}}{\partial W} \tag{26}$$

$$\varepsilon_{\Delta p} = \frac{\partial F_{\mathrm{p}}}{\partial \Delta p} \tag{27}$$

Equation (24) can be rearranged into the following standard form:

$$\mathbf{M}\frac{d\mathbf{y}}{dt} = \mathbf{A}\mathbf{y} \tag{28}$$

The vector **y** contains the small deviations of all the state variables in the system relative to the steady-state:

$$\mathbf{y} = \left[\delta W_1 \quad \delta W_2 \quad \delta W \quad \delta(\Delta p)\right]^{\mathrm{T}} \tag{29}$$

It is important to note that the matrix **M** is a singular matrix. The stability of the system is determined by the eigenvalues λ in the following generalized eigenvalue problem:

$$\lambda \mathbf{M} v = \mathbf{A} v \tag{30}$$

Here, λ represents an eigenvalue, while v is the corresponding eigenvector, which is structured as follows:

$$v = \left[v_{W_1} \quad v_{W_2} \quad v_W \quad v_{\Delta p}\right]^{\mathrm{T}} \tag{31}$$

The stability of the system is determined by the sign of its eigenvalues. If the real part of all eigenvalues is negative, the operating point is stable; conversely, if there exists an eigenvalue with a positive real part, the operating point is unstable.

To evaluate the stability characteristics of the system, the governing equations are reformulated as a eigenvalue problem and solved numerically in MATLAB. For each admissible operating condition, the corresponding eigenvalues and eigenvectors are determined. The stability of the system is then identified from the sign of the computed eigenvalues over the entire operating domain, including all pressure-drop levels and all possible combinations of individual channel flow rates.

Although the present analysis is demonstrated using a system with two parallel channels for clarity, the proposed model and stability analysis method are not limited to two-channel systems. The governing equations are formulated in a general form and can be extended to a system with an arbitrary number of parallel channels by increasing the number of channel momentum equations and applying the overall mass conservation constraint. The eigenvalue-based stability analysis can also be directly applied to multichannel systems, since the system matrices are constructed based on the number of

channels. Therefore, the presented methodology is applicable to parallel microchannel systems with multiple channels commonly encountered in practical applications.

2.5. Model validation

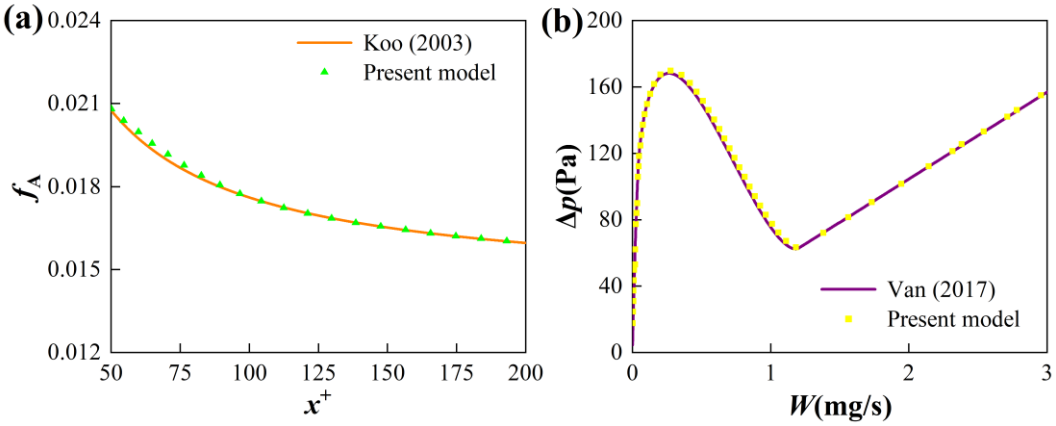

Figure 2. Validation against literature data;
(a) developing-flow friction factor, and
(b) Single-channel pressure drop with fully developed friction factor along the entire channel

To evaluate the reliability of the numerical simulation results in this study, previously published data validated by experimental results were selected for comparative validation. Figure 2(a) compares the developing-flow friction factor, showing that the discrepancy between the present model predictions and the literature data [29] is within 3%. Figure 2(b) presents a comparison of the single channel pressure-drop curves when the fully developed friction factor is applied along the entire channel length, and the deviation between the present model results and the literature data [30] is within 2%. The above comparisons demonstrate that the developed model exhibits high predictive accuracy and good reliability, the numerical simulation results presented in this study are highly credible.

3. Results and discussion

The single-channel pressure-drop curves for a range of the channel length-to-diameter ratio are shown in Figure 3. In each plot, two types are compared: the first type assumes the channel flow does not consider entrance effects, using a fully developed friction factor throughout the entire length; the second type considers entrance effects, with an undeveloped flow region at the inlet where a developing friction factor is used, transitioning to a fully developed friction factor after the entrance region. Purple represents the first type, and blue represents the second type. Solid lines indicate stable operating points, while dashed lines indicate unstable operating points. channel parameters given in Table 1.

Table 1. System Parameters

Parameters	Magnitude		
Channel dimensions: L_c, W_c, H_c (mm)	10 ~ 1250	0.2	0.2
Number of channels	1~2		
Fluid	Water		
Outlet pressure: p_{out} (kPa)	100		
Fluid inlet temperature: T_{in} (K)	353		
Heat source: P_{in} (W)	0.8		

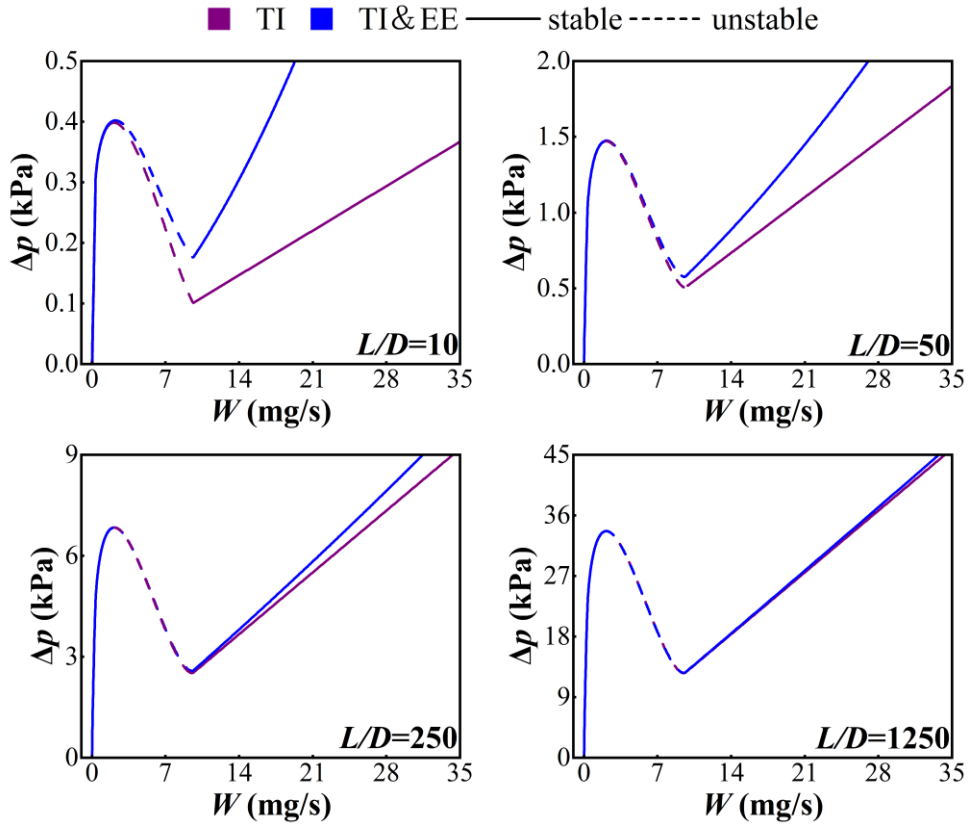

Figure 3. Single-channel pressure-drop curves for a range of different length-to-diameter ratio

Under single-channel heating, the pressure-drop–flow-rate relationship exhibits a non-monotonic N-shaped curve, primarily because variations in mass flow rate alter the extent of phase change. At high flow rates, the fluid remains predominantly single-phase liquid, and the frictional pressure drop increases monotonically with increasing flow rate. As the flow rate decreases to an intermediate range, the heat input per unit mass increases, leading to the onset and intensification of two-phase flow; together with acceleration effects, the effective flow resistance rises markedly, causing the pressure drop to increase as the flow rate decreases. With a further reduction in flow rate, vaporization becomes more severe, the vapor quality increases, and the mixture-averaged density decreases, resulting in a rapid decline in the total pressure drop and ultimately producing the characteristic N-shaped behavior.

The essence of entrance effects is that the boundary layer in the inlet region is not yet fully developed, resulting in a larger near-wall velocity gradient that significantly increases wall shear and, consequently, the frictional pressure drop. Therefore, in the high-flow single-phase liquid regime, where

the pressure drop is dominated by liquid viscous friction, entrance effects introduce a significant additional pressure loss. After the flow enters the two-phase region, the total pressure drop is jointly determined by friction, acceleration, flow regime, and interfacial interactions; the fraction of the total pressure drop attributable to the extra wall friction induced in the entrance region decreases, so the overall pressure-drop enhancement becomes relatively limited. In the vapor-dominated regime, gas viscosity is low and the frictional pressure drop is inherently small, making the total pressure drop much less sensitive to entrance-region friction; hence, the contribution of entrance effects is nearly negligible.

As the channel length-to-diameter ratio increases, the entrance region accounts for a progressively smaller fraction of the total channel length, and thus the influence of entrance effects becomes increasingly weak. As shown in Figure 3, with increasing length-to-diameter ratio, the pressure-drop curves obtained with and without entrance effects approach each other. When the channel is sufficiently long, the entrance-region contribution becomes negligible compared with the overall frictional pressure drop, and the entrance effect can be safely ignored.

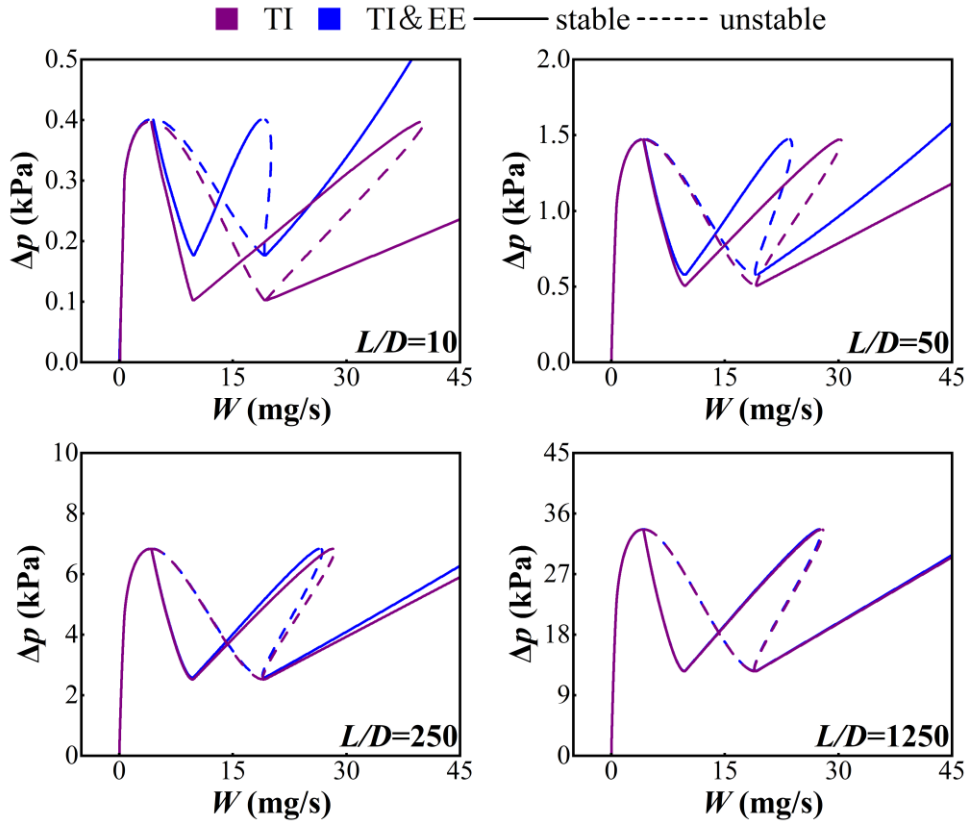

Figure 4. Two-channel pressure-drop curves for a range of different length-to-diameter ratio

Because the single channel pressure drop-flow rate relationship exhibits a nonmonotonic N shaped behavior, up to three flow rates can correspond to the same pressure drop. In a parallel two channel system, the channels share common inlet and outlet manifolds and must sustain the same pressure drop. Therefore, under a given pressure drop, the two channels can form 3^2 possible flow rate combinations, giving rise to multiple system pressure drop curves associated with uniform and nonuniform flow distributions. In the cumulative pressure drop curve of two parallel channels, the same total flow rate may correspond to multiple pressure drop values. This phenomenon arises from the fact that, in the pressure drop curve of a single channel, the region with a negative slope corresponds to the

unstable two-phase flow regime. In a system of two parallel channels, when one channel operates in the two-phase flow region, a small perturbation that reduces the flow rate in this channel will cause an increase in its pressure drop due to the negative slope characteristic. Under the condition of constant total flow rate and equal pressure drop between parallel channels, the flow rate in the other channel must increase to maintain pressure equilibrium. If the other channel operates in the liquid phase, its pressure drop increases with increasing flow rate. Since the slope of the pressure drop curve in the two-phase region is steeper than that in the liquid phase, the pressure increase in the liquid channel is insufficient to compensate for the pressure rise in the two-phase channel. As a result, the flow rate in the two-phase channel continues to decrease, while the flow rate in the liquid channel continues to increase, leading to flow maldistribution until a new equilibrium is reached. This mechanism fundamentally explains the occurrence of Ledinegg instability in parallel channel systems.

As shown in Figure 4, when the channel length-to-diameter ratio increases, the entrance effect weakens and the two-channel pressure drop curves with and without entrance effects gradually converge, so the entrance effect can be neglected for sufficiently long channels. When the channel length-to-diameter ratio decreases, the entrance effect becomes stronger and the instability range indicated by the dashed segment is markedly reduced when entrance effects are included.

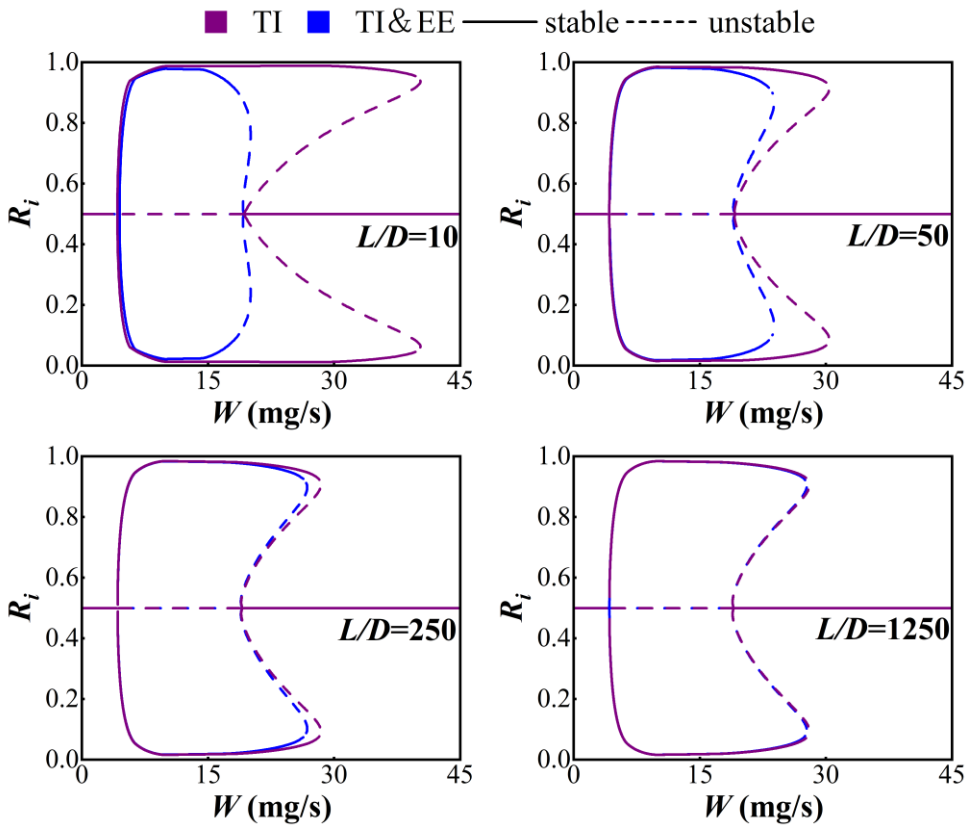

Figure 5. Two-channel flow distribution for a range of different length-to-diameter ratio

Figure 5 shows the flow distribution in the two-channel system, where the sum of the flow rate fractions R_i of the two channels equals 1. When flow maldistribution occurs, channel 1 is assumed to carry a higher flow rate while channel 2 carries a lower flow rate. Owing to entrance effects, the higher flow rate in channel 1 corresponds to a larger liquid fraction, whereas the lower flow rate in channel 2 corresponds to a

smaller liquid fraction. As a result, entrance effects increase the pressure drop in channel 1 more significantly, leading to a larger hydraulic resistance. This promotes flow redistribution toward channel 2 and thus alleviates flow maldistribution between the two channels. As the channel length-to-diameter ratio increases, the entrance effect weakens and the flow distribution curves with and without entrance effects gradually converge. Conversely, as the channel length-to-diameter ratio decreases, the entrance effect becomes stronger and the flow maldistribution is further mitigated when entrance effects are taken into account.

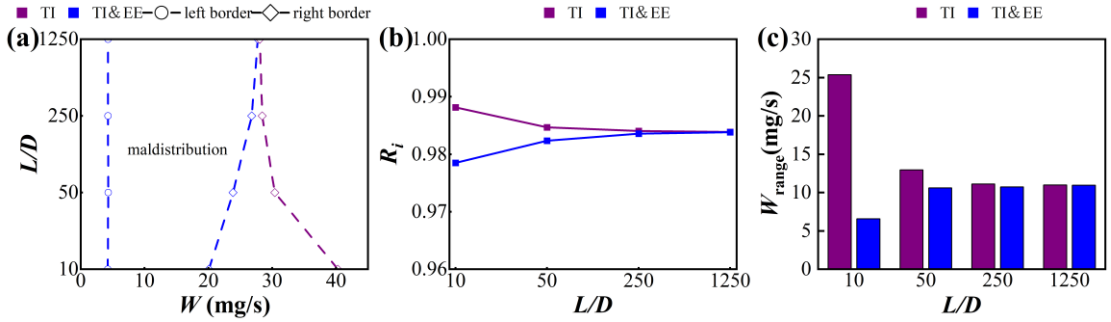

Figure 6. Two-channel flow maldistribution for a range of different length-to-diameter ratio;
(a)the range of total flow rates over which maldistribution occurs,
(b)the most severe flow maldistribution, and
(c)the range of total flow rates with this most severe flow maldistribution

Figure 6 illustrates how flow maldistribution in the two-channel system varies with the channel length-to-diameter ratio. Figure 6(a) As the channel length-to-diameter ratio increases, the entrance effect gradually weakens, leading to a reduction in its flow-equalizing influence, and the maldistribution range obtained with and without entrance effects gradually converges. Figure 6(b) With increasing length-to-diameter ratio, the most severe maldistribution under the two conditions progressively becomes consistent, as reflected by the convergence of the flow rate fraction in the high flow channel 1. Figure 6(c) Similarly, as the channel length-to-diameter ratio increases, the total flow rate interval associated with the most severe maldistribution in the two cases gradually coincides; when the channel length-to-diameter ratio decreases, entrance effects further shrink this total flow rate interval.

4. Conclusion

This paper presents a parallel microchannel two-phase flow model that accounts for the entrance effect and examines its impact on flow instability and distribution. The study highlights the role of the channel length-to-diameter ratio in this process. The results show that the entrance effect promotes flow redistribution by increasing the frictional pressure drop in high-flow channels. Notably, as the channel length-to-diameter ratio decreases, the impact of the entrance effect becomes more significant, whereas as the ratio increases, the effect diminishes and can eventually be neglected. These findings provide valuable theoretical insights for the design of microchannel heat sinks, enhancing their stability and guiding their geometric optimization.

Nomenclature

A_c — channel cross-section area, [mm²]
A — linearized system matrix, [–]
C — Chisholm constant, [–]
D_h — hydraulic diameter, [mm]
$F_p(W, \Delta p)$ — pump curve, [–]
F_w — volumetric wall shear force, [N]
f — friction factor, [–]
$f(W)$ — channel load curve, [–]
G — mass flux, [kg/(m²-s)]
H_c — channel height, [mm]
h — specific enthalpy, [J/kg]
L_c — channel length, [mm]
M — mass matrix, [–]
m — channel inertial coefficient, [–]
N — number of parallel channels, [–]
$P_{[0,1]}$ — projection on the interval [0, 1] , [–]
p — pressure, [kPa]
Δp— pressure drop, [kPa]
P_{in} — heat input, [W]
Re — Reynolds number, [–]
R_i — flow rate fraction, [–]
S — slip ratio, [–]
T — temperature, [K]
t — time coordinate, [s]
u — streamwise velocity, [m/s]
v — specific volume, [kg/m³]
$\boldsymbol{v}$ — eigenvector, [–]
W — flow rate, [kg/s]
W_c — channel width, [mm]
x — vapor quality, [–]
y — vector of state variables, [–]
z — streamwise coordinate, [mm]

Greek symbols

α — void fraction, [–]
β — aspect ratio, [–]
ε — partial derivative, [–]
δ — deviation, [–]
γ — relative finite difference step size, [–]
λ — eigenvalue, [–]
μ — dynamic viscosity, [kg/m-s]

Subscript

c — channel, [–]
f — liquid, [–]
g — vapor, [–]
i — channel index, [–]
in — inlet, [–]
out — outlet, [–]
sat — saturation, [–]

References

[1] U. Ghani, M.A. Wazir, K. Akhtar, M. Wajib, S. Shaukat, Microchannel heat sinks—A comprehensive review, *Electronic Materials 5(4)* (2024) 249–292.

[2] Y. Fu, G. Shan, X. Zhang, L. Zhao, Y. Yang, Design and fabrication of embedded microchannel cooling solutions for high-power-density semiconductor devices, *Micromachines 16(8)* (2025) 908.

[3] D. Dai, J. Zhu, H. Li, S. Ma, H. Lv, Q. Lv, Numerical investigation of heat transfer performance in parallel and symmetric wavy microchannel heat sinks, *Thermal Science (00) (2025)* 134–134.

[4] B.J. Jones, P.-S. Lee, S.V. Garimella, Infrared micro-particle image velocimetry measurements and predictions of flow distribution in a microchannel heat sink, *International Journal of Heat and Mass Transfer 51(7)* (2008) 1877–1887. https://doi.org/https://doi.org/10.1016/j.ijheatmasstransfer.2007.06.034.

[5] J. Mathew, P.-S. Lee, T. Wu, C.R. Yap, Experimental study of flow boiling in a hybrid microchannel-microgap heat sink, *International Journal of Heat and Mass Transfer 135* (2019) 1167–1191. https://doi.org/https://doi.org/10.1016/j.ijheatmasstransfer.2019.02.033.

[6] L. Cheng, G. Xia, Fundamental issues, mechanisms and models of flow boiling heat transfer in microscale channels, *International Journal of Heat and Mass Transfer 108* (2017) 97–127. https://doi.org/https://doi.org/10.1016/j.ijheatmasstransfer.2016.12.003.

[7] S. Nemoda, M. Paprika, M.R. Mladenović, A.D. Marinković, G.S. Živković, Two-dimensional mathematical model of liquid fuel combustion in bubbling fluidized bed applied for a fluidized furnace numerical simulation, *Thermal Science 22(2)* (2018) 1121 – 1135.

[8] M.M. Petrovic, V.D. Stevanovic, Two-component two-phase critical flow, *FME Transactions 44(2)* (2016) 109–114.

[9] A.D. Stojanović, S.V. Belošević, N.Đ. Crnomarković, I.D. Tomanović, A.R. Milićević, Nucleate pool boiling heat transfer: Review of models and bubble dynamics parameters, *Thermal Science 26(1 Part A)* (2022) 157 – 174.

[10] M. Pezo, V.D. Stevanovic, Z. Stevanovic, A two-dimensional model of the kettle reboiler shell side thermal-hydraulics, *International journal of heat and mass transfer 49(7-8)* (2006) 1214–1224.

[11] I. Tomanović, S. Belošević, A. Milićević, N. Crnomarković, A. Stojanović, L. Deng, D. Che, CFD Code Parallelization on GPU and the Code Portability, *Advanced Theory and Simulations 8(3)* (2025) 2400629.

[12] M.L. Pezo, V.D. Stevanović, Numerical prediction of nucleate pool boiling heat transfer coefficient under high heat fluxes, *Thermal Science 20* (2016) S113 – S123.

[13] M. Pezo, V. Stevanovic, Numerical prediction of critical heat flux in pool boiling with the two-fluid model, *International Journal of Heat and Mass Transfer 54(15-16)* (2011) 3296–3303.

[14] M.R. Mladenović, S. Nemoda, M. Paprika, A.D. Marinković, Application of analytical and CFD models of liquid fuels combustion in a fluidized bed, *Thermal Science 23(Suppl. 5)* (2019) 1627 – 1636.

[15] W. Fang, J. Sang, H. Li, S. Yin, Y. Huang, Development of hydrodynamic and thermal boundary layer in the entrance region with hydrophobic surfaces, *International Journal of Heat and Mass Transfer 253* (2025) 127618.

[16] Z. Duan, H. Ma, Pressure drop and heat transfer in the entrance region of microchannels, in: Advances in Heat Transfer, Elsevier2020, pp. 249–333.

[17] Y.H. Soo, K.H. Yu, M.A. Ismail, Heat transfer enhancement of microchannel heat sink with water-droplet grooves: geometrical and grooves arrangement effects, *Journal of the Brazilian Society of Mechanical Sciences and Engineering 47(11)* (2025) 568.

[18] G. Gamrat, M. Favre-Marinet, D. Asendrych, Conduction and entrance effects on laminar liquid flow and heat transfer in rectangular microchannels, *International Journal of Heat and Mass Transfer 48(14)* (2005) 2943–2954. https://doi.org/https://doi.org/10.1016/j.ijheatmasstransfer.2004.10.006.

[19] G. Ferreira, A. Sucena, L.L. Ferrás, F.T. Pinho, A.M. Afonso, Hydrodynamic entrance length for laminar flow in microchannels with rectangular cross section, *Fluids 6(7)* (2021) 240.

[20] G.L. Morini, Single-phase convective heat transfer in microchannels: a review of experimental results, *International journal of thermal sciences 43(7)* (2004) 631–651.

[21] W. Qu, I. Mudawar, Analysis of three-dimensional heat transfer in micro-channel heat sinks, *International Journal of heat and mass transfer 45(19)* (2002) 3973–3985.

[22] S. Kandlikar, Heat transfer and fluid flow in minichannels and microchannels, elsevier2006.

[23] S.M. Zivi, Estimation of steady-state steam void-fraction by means of the principle of minimum entropy production, (1964).

[24] W.R. Lockhart, Proposed correlation of data for isothermal two-phase, two-component flow in pipes, *Chemical engineering progress 45(1)* (1949) 39–48.

[25] D. Chisholm, A theoretical basis for the Lockhart-Martinelli correlation for two-phase flow, *International Journal of Heat and Mass Transfer 10(12)* (1967) 1767–1778.

[26] Y.S. Muzychka, M.M. Awad, Asymptotic generalizations of the Lockhart–Martinelli method for two phase flows, (2010).

[27] R.K. Shah, A.L. London, Laminar flow forced convection in ducts: a source book for compact heat exchanger analytical data, Academic press2014.

[28] R.K. Shah, A correlation for laminar hydrodynamic entry length solutions for circular and noncircular ducts, (1978).

[29] J. Koo, C. Kleinstreuer, Liquid flow in microchannels: experimental observations and computational analyses of microfluidics effects, *Journal of Micromechanics and Microengineering 13(5)* (2003) 568.

[30] T. Van Oevelen, J.A. Weibel, S.V. Garimella, Predicting two-phase flow distribution and stability in systems with many parallel heated channels, *International Journal of Heat and Mass Transfer 107* (2017) 557–571.

Paper submitted: 21 February 2026
Paper revised: 09 April 2026
Paper accepted: 14 April 2026